HHS Public Access

Author manuscript

*J Acquir Immune Defic Syndr*. Author manuscript; available in PMC 2021 February 24.

Published in final edited form as:

*J Acquir Immune Defic Syndr*. 2020 August 01; 84(4): 414–421. doi:10.1097/QAI.0000000000002360.

# Machine Learning Analysis Reveals Novel Neuroimaging and Clinical Signatures of Frailty in HIV

**Robert H. Paul, PhD**[a,b], **Kyu S. Cho, MS**[b], **Patrick Luckett, PhD**[c], **Jeremy F. Strain, PhD**[c], **Andrew C. Belden, PhD**[b], **Jacob D. Bolzenius, PhD**[b], **Jaimie Navid, BA**[c], **Paola M. Garcia-Egan, MS**[a,b], **Sarah A. Cooley, PhD**[c], **Julie K. Wisch, PhD**[c], **Anna H. Boerwinkle, BS**[c], **Dimitre Tomov, MS**[c], **Abel Obosi, PhD**[b,d], **Julie A. Mannarino, BA**[b], **Beau M. Ances, MD, PhD**[c]

[a]Department of Psychological Sciences, University of Missouri, Saint Louis, MO;

[b]Missouri Institute of Mental Health, University of Missouri, Saint Louis, MO;

[c]Department of Neurology, Washington University School of Medicine, Saint Louis, MO;

[d]Department of Psychology, University of Ibadan, Ibadan, Nigeria.

## Abstract

**Background:** Frailty is an important clinical concern for the aging population of people living with HIV (PLWH). The objective of this study was to identify the combination of risk features that distinguish frail from nonfrail individuals.

**Setting:** Machine learning analysis of highly dimensional risk features was performed on a clinical cohort of PLWH.

**Methods:** Participants included 105 older (average age = 55.6) PLWH, with at least a 3-month history of combination antiretroviral therapy (median CD4 = 546). Predictors included demographics, HIV clinical markers, comorbid health conditions, cognition, and neuroimaging (ie, volumetrics, resting-state functional connectivity, and cerebral blood flow). Gradient-boosted multivariate regressions were implemented to establish linear and interactive classification models. Model performance was determined by sensitivity/specificity (F1 score) with 5-fold cross validation.

**Results:** The linear gradient-boosted multivariate regression classifier included lower current CD4 count, lower psychomotor performance, and multiple neuroimaging indices (volumes, network connectivity, and blood flow) in visual and motor brain systems (F1 score = 71%; precision = 84%; and sensitivity = 66%). The interactive model identified novel synergies between neuroimaging features, female sex, symptoms of depression, and current CD4 count.

Correspondence to: Robert H. Paul, PhD, University of Missouri, St. Louis, 4633 World Parkway Circle, St. Louis, MO 63141 (paulro@umsl.edu).

The authors have no conflicts of interest to disclose.

Supplemental digital content is available for this article. Direct URL citations appear in the printed text and are provided in the HTML and PDF versions of this article on the journal's Web site (www.jaids.com).

**Conclusions:** Data-driven algorithms built from highly dimensional clinical and brain imaging features implicate disruption to the visuomotor system in older PLWH designated as frail individuals. Interactions between lower CD4 count, female sex, depressive symptoms, and neuroimaging features suggest potentiation of risk mechanisms. Longitudinal data-driven studies are needed to guide clinical strategies capable of preventing the development of frailty as PLWH reach advanced age.

**Keywords**

HIV; frailty; machine learning; neuroimaging

## INTRODUCTION

The life-preserving benefits of combination antiretroviral therapy (cART) have shifted the global HIV epidemic toward an older demographic. Although the first reported cases of HIV in the United States involved young adult males, the average age of the US population is now older than 50 years of age.[1] A similar trend is occurring worldwide in conjunction with improved access to cART and associated follow-up medical care for people living with HIV (PLWH) which have significantly lowered HIV-related mortality.[1] Increased life expectancy among PLWH introduces new health challenges related to age-related conditions that affect PLWH at younger ages and with greater severity when compared with age-similar uninfected individuals.[2,3]

Frailty, a state of significant health vulnerability,[4] was identified as a complication of untreated HIV during the early years of the HIV epidemic. In the current era of suppressive cART, frailty has re-emerged as a relevant clinical concern for individuals who are living into advanced ages.[5] Recent studies using the Fried phenotype criteria[4] (reduced ambulation/motor speed, physical weakness, unintended weight loss, exhaustion, and/or reduced activity level) report a higher prevalence, incidence, and earlier age of frailty onset in PLWH compared with demographically similar uninfected comparisons.[5,6] Risk factors reported in previous studies include more severe HIV disease indices (eg, higher viral load, lower CD4 count, and elevated plasma markers of immune activation),[2,6,7] female sex,[5,6] and coexisting health complications, such as hepatitis C virus (HCV),[2] depression,[5–7] chronic obstructive pulmonary disease,[6] and diabetes.[2,6]

Neuroimaging and cognitive signatures of frailty in PLWH are less well known. A preliminary study[8] of individuals defined as “prefrail” described associations between select subcortical brain volumes (eg, putamen) and motor components of the frailty phenotype[4] (eg, slow motor speed), but the direction of associations was not consistent across brain regions. Furthermore, the overlap between symptoms of frailty and neurobehavioral features of HIV is difficult to distinguish using traditional analytic strategies.[9]

A recent study by our group[10] used deep learning to establish classifiers of the frailty phenotype and cognitive symptoms of HIV using regional cerebral blood flow (CBF). The data-driven algorithm distinguished frail from nonfrail PLWH (accuracy of 75%) using CBF values derived from subcortical brain regions (ie, pallidum, amygdala, caudate, hippocampus, and thalamus) and CBF in the cerebellum. These findings suggest that frailty

in older PLWH receiving cART represents alterations in multiple brain regions. The objective of this study was to identify the combination of demographic, HIV clinical, and brain/structure features that distinguish frail from nonfrail PLWH in the context of cART.

## METHODS

### Study Participants

Participant characteristics are listed in Table 1. PLWH were recruited from ongoing studies at Washington University in Saint Louis (WUSTL) Infectious Disease Clinic and the WUSTL AIDS Clinical Trial Unit (ACTU). Inclusion criteria were as follows: ≥40 years of age, ≥8 years of education, ability to provide informed written consent, English as the primary language, and use of cART for at least 3 months. Individuals were excluded if they reported head injury with loss of consciousness >30 minutes, active psychosis, severe symptoms of anxiety or depression, opportunistic infection, or problematic alcohol/substance use. The study was approved by the affiliated institutional review boards. Participants received financial compensation for their time.

### Frailty Assessment

Individuals were designated as frail or nonfrail according to the Fried phenotype criteria[4] if they had at least 3 of the following: (1) unintended weight loss, (2) exhaustion, (3) low activity levels, (4) gross motor slowness, and/or (5) weakness. Participants who endorsed fewer than 3 of these symptoms were defined as nonfrail (n = 54), consistent with previous work.[5]

### Predictor Variables

**Demographics—**Age, sex, years of education, and ethnicity.

**HIV Disease—**Current and nadir CD4 T-cell count and current plasma viral load recorded from medical records within 3 months of the other assessments.

**Health Comorbidities—**Symptoms of depression [Beck Depression Inventory-II (BDI-II) affective subscale],[11] HCV coinfection, diabetes, and self-reported substance use.

**Cognitive Performance—**Participants completed cognitive tests of psychomotor speed, learning and memory, executive function, and language.

Psychomotor speed: Trail Making Test A (Trails A)[12] required participants to draw a line as quickly as possible to connect circles numbered from 1 to 25 scattered on the test page; Digit Symbol[13] required individuals to associate symbols corresponding to specific numbers using a key in written format; Grooved Pegboard[14] required individuals to insert pegs into holes aligned in different directions; Symbol Search[13] required identification of target symbols among foils; and Learning and Memory: Verbal learning and memory were examined using the Hopkins Verbal Learning Test—Revised (HVLT-R),[15] which required participants to learn 12 words over 3 learning trials. Free recall was tested after a 20-minute delay; visual learning and memory were tested with the Brief Visuospatial Memory Test—

Revised (BVMT-R),[16] which required individuals to learn and remember 6 geometric designs presented over 3 learning trials. Free recall was tested after a 20-minute delay. Executive function: Color-Word Interference Test (CWIT-3)[17] required individuals to name words printed in incongruent ink; verb fluency[18] required generation of action words as quickly as possible for 60 seconds; Trail Making Test B (TrailsB)[12] required individuals to connect circles alternating in ascending order between numbers and letters; Letter Number Sequencing (LNS)[13] required participants to recall a string of letters and numbers in numeric and alphabetical order. Language: Letter fluency (FAS)[19] required individuals to provide verbal exemplars of words that begin with F, A, and then S as quickly as possible for 60 seconds without use of proper nouns; category fluency[20] required verbal generation of animals. Raw scores were converted to standardized scores (Z-scores) using published norms[13,21,22]; domain scores were averaged to create an overall score.

**Multimodal Neuroimaging—**Neuroimaging was acquired using high resolution 3T MRI (Siemens Tim Trio; Siemens AG, Erlangen, Germany). The protocol included structural T1-weighted (T1w) and T2-weighted (T2w), resting-state blood oxygen level–dependent functional MRI (rs-fcMRI), and pseudocontinuous arterial spin labeling (pCASL) sequences. For all scanning parameters, a 12-channel head coil was applied. The T1w structural scans used a 3-dimensional, sagittal, magnetization-prepared rapid gradient-echo (MP-RAGE) sequence with repetition time (TR) = 2400 ms, echo time (TE) = 3.16 ms, flip angle = 8°, inversion time = 1000 ms, voxel size = 1 × 1 × 1 $mm^3$ voxels, 256 × 256 × 176 acquisition matrix, and 162 slices.

A three-dimensional T2w fast spin-echo scan (TE = 450 ms, TR = 3,200 ms, 256 × 256 × 176 acquisition matrix, and 1 × 1 × 1 $mm^3$ voxels) was acquired for image registration. Resting-state fMRI scans were collected using a gradient spin-echo sequence (TE = 27 ms, TR = 2.2 seconds, 64 × 64 acquisition matrix, and flip angle = 90°). Two resting-state functional connectivity scans were acquired. Participants remained in the supine position and were instructed to fixate on a cross-hair presented visually. CBF was derived from pCASL arterial spin labeling using the following sequence:1.5-second labeling time, 1.2-second postlabeling delay, TR of 3,500 ms, TE of 9.0 ms, 64 × 64 acquisition matrix, 90° flip angle, 22 axial slices with a 1-mm gap, and voxel size of3.4 × 3.4 × 5.0. Two pCASL scans were acquired, each containing 60 volumes (30 pairs of control and label volumes and a duration of 3.5 minutes).

Brain segmentation and parcellation of the structural images were obtained using the FreeSurfer software suite (v5.3) (Martinos Center, Harvard University, Boston, MA). Each participant map was visually inspected by a trained research technician and corrected if necessary. The echoplanar (EPI) pCASL images were registered to a common template through a combined affine transformation (EPI ⟶ T2w ⟶ T1w ⟶ atlas).[23] CBF values were computed for each control–label pair using a single compartment model, as previously described.[10] Spatial smoothing was conducted using a Gaussian kernel (FWHM = 10 mm). The temporal derivative of variance (DVARS) was used to calculate weights for each control–label pair. Subsequently, weighted-CBF volumes were averaged to calculate mean weighted-CBF.[23] Parcellated structural images were used to obtain CBF measures from 82 cortical and subcortical gray matter brain regions, as defined by the Desikan–Killiany atlas.

Analyses of resting-state functional connectivity (rs-fcMRI) were performed as previously described.[24] Echoplanar imaging (EPI) distortion due to magnetization inhomogeneity was corrected using a mean field map method.[25] The rs-fcMRI scans were registered to a common template through combined transformation (EPI ⟶ T2w ⟶ T1w ⟶ atlas). Motion correction eliminated frames according to DVARS and frame displacement.[26] Signals originating from nongray matter tissue were treated as nuisance regressors derived from white matter, ventricles, and the extra-axial space that were all segmented using FreeSurfer. Additional regressors included parameters derived from rigid body head motion correction, average global signal, and global signal temporal derivative. Regional averages were extracted for each volume.[27] Preprocessed BOLD time series were extracted from 298 regions of interest and partitioned into 13 standard networks: sensorimotor (SM), lateral sensorimotor, cingulate operculum, auditory (AUD), default mode (DMN), parietal memory (MEM), visual (VIS), frontal parietal (FP), salience (SAL), subcortical (SUB), cerebellum (CEREB), ventral attention (VAN), and dorsal attention (DAN). Average connectivity was computed for within and between networks, resulting in a 13 × 13 network matrix. Each cell of the matrix located in the upper triangle was included in the model as the correlation between the given networks.

## Machine Learning Approach

Gradient-boosted multivariate regression (GBM)[9] was used to build the classification models. GBM is a form of ensemble machine learning that uses a “wisdom of crowds” approach to optimize accuracy and minimize error.[9] Recent studies from our team and by others have successfully deployed ensemble machine learning to establish novel explanatory models of complex clinical phenotypes, including neurodevelopment in children with perinatal HIV infection,[28] posttraumatic stress disorder,[29] and probable Alzheimer disease.[30]

## Feature Selection and Model Performance

Consistent with our previous work,[28] feature selection was conducted using an in-house program based on SciKit[31] and PDPBox.[32] Class labels (frail vs. nonfrail) were determined using a probability score based on the sigmoid function $(1/(1+\hat{e}(-x)))$, with a 0.5 decision boundary and application of gradient descent to minimize error. The final set of features included >1100 data elements. Model performance was defined using the F1 score, which represents the harmonic balance between precision (ie, positive predictive value) and sensitivity (ie, proportion of true positives identified correctly). The F1 score is appropriate for unbalanced designs that are prone to inflate model performance when examined using accuracy derived from receiver operator curves (ie, accuracy paradox).[33] Separate GBMs were implemented to establish classification algorithms built from linear vs. interactive features.

## Model Stability and Validation

Several steps were implemented to support internal and external validity. First, as noted above, the algorithms were built using a machine learning method that minimizes error and overfitting by leveraging results from multiple individual models.[9] Second, we trained and tested the algorithms on 10 features with the strongest classification values (ie, mutual

information criterion). Setting the feature list to a maximum of 10 predictors reduces overfitting while enhancing model interpretation.[9] Finally, we used 5-fold cross validation (25 total validation trials) to calculate the average F1 score as the final measure of model performance.

### Additional Analyses

Results from the GBM analyses were compared with outcomes obtained through logistic regression. Logistic regression uses iterative learning to build linear models from predictors that have been determined in advance and included as independent variables in the model. To facilitate the comparison with GBMs, we built logistic regression algorithms using a 2-step procedure; the first step ranked the relative importance of features according to posterior probabilities, and the second step examined the average F1 score using the 10 input features with the highest coefficient strengths identified in the first step.

## RESULTS

### Demographic and Clinical Comparisons

Participants included 105 individuals with chronic HIV. Demographics and HIV clinical characteristics are provided in Table 1. In brief, the sample predominately comprised African American (60%) men (85%), with a mean age of 55.6 (SD = 7.4) and a median CD4 T-cell count of 546 cells/mm$^3$; 70% were virally suppressed, defined as viremia <20 copies/mL. Comparisons between frail and nonfrail PLWH revealed no significant differences in age, race, or education ($P$s > 0.05). The proportion of women in the frail group was higher than that in the nonfrail group ($P < 0.05$). The duration of HIV infection and viral detectability were similar between the 2 groups ($P > 0.05$). By contrast, the nadir CD4 count and the current CD4 count were higher in frail individuals ($P < 0.05$), although current CD4 was relatively high in both groups (>500 cells/mm$^3$). Frail individuals reported more depressive symptoms than individuals in the nonfrail group ($P < 0.05$). HCV was nearly twice as common in frail individuals, but the difference was not statistically significant ($P >$ 0.05). Similarly, average domain-specific and overall neurocognitive performances did not differ between groups ($P$s >0.05).

### Machine Learning Classification of Frailty Without Interactions

The linear GBM classified PLWH as frail or nonfrail individuals with an F1 score of 71% (precision = 84% and sensitivity = 66%, averaged across the 25 validation trials). Ranked by relative importance (Fig. 1), the model comprised the following: **feature 1)** reduced CBF in the right pallidum, **feature 2)** reduced CBF in the left occipital cortex, **feature 3)** lower psychomotor performance, **feature 4)** reduced volume of the right pericalcarine region, **feature 5)** lower rs-fcMRI between the FP and VAN, **feature 6)** lower rs-fcMRI between the VIS and DAN, **feature 7)** lower recent CD4, **feature 8)** lower rs-fcMRI between the MEM and CEREB, **feature 9)** lower intranetwork rs-fcMRI in the DAN, and **feature 10)** lower volume of the right pars triangularis. Collectively, the predictors selected by the data-driven algorithm represent components of visuomotor brain systems (see Fig. 2).[34]

### Machine Learning Classification of Frailty With 2-Way Interactions

The GBM allowing 2-way interactions yielded a similar classification performance (F1 score of 71% [precision = 89% and sensitivity = 64%, averaged across the 25 validation trials]) (Figs. 3 and 4). The algorithm included 9 interactive features (denoted as feature pairs) and 1 linear feature (symptoms of depression). **Feature pair 1)** higher symptoms of depression with lower rs-fcMRI between the SAL and SUB, **feature pair 2)** higher symptoms of depression, **feature pair 3)** lower rs-fcMRI between the FP and SAL with lower rs-fcMRI between the SAL and SUB, **feature pair 4)** lower volume of the right isthmus of the cingulate and lower volume of the left thalamus, **feature pair 5)** lower rs-fcMRI between the DMN and DAN and lower volume in the right superior-parietal region, **feature pair 6)** lower recent CD4 and lower brainstem volume, **feature pair 7)** lower rs-fcMRI between the DMN and CEREB with lower rs-fcMRI between the VIS and SAL, **feature pair 8)** lower volume of the left postcentral gyrus and female sex, **feature pair 9)** lower volume in the right pericalcarine region and lower volume of the right precentral gyrus, and **feature pair 10)** lower rs-fcMRI between the SM and FP and lower intra-rs-fcMRI in the SUB.

### Logistic Regression

Logistic regression yielded an average F1 score of 57% (precision = 69% and sensitivity = 53%, averaged across validation trials). The predictive features in the logistic regression algorithm are provided in Supplemental Digital Content 1, http://links.lww.com/QAI/B458. As expected, classification performance obtained through logistic regression was markedly lower than that obtained through the GBM models.

## DISCUSSION

The study findings provide the first data-driven model of frailty in older PLWH. Features derived from multimodal neuroimaging, neurocognitive testing (psychomotor speed), and CD4 T-cell count collectively differentiated frail individuals from nonfrail individuals with chronic HIV. Each neuroimaging modality (volumes, rs-fcMRI, ASL) contributed to the classification performance; however, alterations in both internetwork and intranetwork connectivity defined by rs-fcMRI were more heavily represented in the final algorithm. Furthermore, neuroimaging and neurocognitive testing results suggest that frailty in older PLWH reflects disruption to visuomotor network integrity. Finally, interdependencies between brain measures, ongoing immune suppression, female sex, and symptoms of depression indicate putative synergies across risk mechanisms. Taken together, results from our ensemble machine learning model advance the conceptual framework of frailty among older PLWH receiving cART and point toward possible clinical strategies to improve long-term health in this population.

Reduced CBF in the pallidum was the strongest classification feature of frailty in the linear GBM model. This finding is consistent with results from our recent analysis of the cohort using deep learning[10] and a large body of evidence, implicating the pallidum as a key determinant of motor problems associated with PLWH.[35] Brain volumetric data highlighted the right pars triangularis, which is particularly interesting considering the role of the left pars triangularis in language tasks. By contrast, task-based functional MRI reveals activation

of the right pars triangularis during imagined movement, which has been attributed to inhibitory networks.[36] The strong relevance of motor brain regions (cerebellum, subcortical, and supplemental motor) identified in the GBM models aligns with the recent suggestion by Morgello et al[6] that frailty in PLWH corresponds to damage in cerebral mechanisms important for motor function.

The second strongest classification feature identified in our linear GBM included CBF in the occipital lobe. Additional evidence implicating visual brain systems in the expression of frailty among PLWH includes the observation that pericalcarine volume and VIS connectivity were strong classifiers in the GBM model. Although primary visual impairment (eg, blindness) is not typical of HIV-related brain injury, a compelling body of evidence from previous neuroimaging studies indicates that the occipital cortex is not spared among PLWH, including individuals receiving cART.[37,38] For example, Ances et al[37] reported reduced occipital CBF in a separate cohort of young adults with HIV, suggesting that networks innervating the visual cortex are disrupted before individuals reach an advanced age. This is consistent with the observation that age-related health comorbidities in the era of cART are observed more in PLWH at younger ages than their uninfected counterparts.[2,3]

The observation that psychomotor speed emerged as the only cognitive classifier is interesting because this domain was defined in the current study by individual tests that require online integration of visually guided motor behavior (ie, Trails A,[12] Digit Symbol,[13] Grooved Pegboard,[14] and Symbol Search[13]). By contrast, the other domains (ie, learning and memory, executive function, and language) were at least partially comprised tests that do not require visual and/or motor function. Our machine learning approach also revealed alterations in brain networks (ie, resting state connectivity) in the VIS, a brain region that receives substantial input from brain regions required for successful navigation of the physical environment.[39] Conceptually, the data-driven results described in this study provide empirical support for the recent proposal by Morgello et al[6] that frailty in PLWH results from damage to white matter pathways critical for cognitive and motor function. Future studies are needed to determine the earliest neuroimaging signatures of frailty and whether subsequent changes to brain structure and function unfold sequentially—a potentially transformative opportunity to intervene before the onset of clinical symptoms.

Most participants included in this study had a CD4 cell count >500 cells/mm$^3$; yet, the interactive GBM revealed a synergy between lower CD4 T-cell count and regional brain volume as an interactive risk feature for frailty. Caution is warranted about overinterpretation of this finding, but it is noteworthy that persistent immune dysregulation is believed to underlie chronic disease comorbidity among individuals taking suppressive cART.[40] For example, recent work from the AIDS Clinical Trials Group[41] describes residual HIV DNA in the CSF among cognitively impaired PLWH with a peripheral viral load <100 copies/mL. Although previous studies describe the lower limit of viremia associated with HIV transmission,[42,43] our results reinforce the need to empirically define the threshold of disease activity and immune suppression that informs subsequent risk of emergent health consequences. In addition, because our study focused on CD4 count as the primary immune marker, there is a need to explore a larger array of immune markers (eg, neopterin, soluble CD163, and CD4/CD8 ratio) as potential predictive classifiers of frailty. Finally, longitudinal

studies are needed to define the causal pathways underlying interactions between depressive symptoms, female sex, and prevalent health conditions such as HCV on frailty risk in PLWH receiving long-term cART. Results from this study provide an important first step toward data-informed clinical strategies capable of preventing the development of frailty as PLWH reach advanced age.

## Supplementary Material

Refer to Web version on PubMed Central for supplementary material.

## ACKNOWLEDGMENTS

The authors are grateful to the study participants and the research team members for their support.

Supported by the National Institutes of Health [R01 NR012657 and R01 NR014449], the National Institute of Mental Health [R01 MH114722], the U.S. Army Medical Research Acquisition Activity [W81XWH-11-2-0174], and the Fogarty International Center of the National Institutes of Health [D43TW009608].

## REFERENCES

1. Joint United Nations Programme on HIV/AIDS. HIV and Aging. 2013 Available at: http://www.unaids.org/en/media/unaids/contentassets/documents/unaidspublication/2013/20131101_JC2563_hiv-and-aging_en.pdf. Accessed December 3, 2019.
2. Erlandson KM, Schrack JA, Jankowski CM, et al. Functional impairment, disability, and frailty in adults aging with HIV-infection. Curr HIV/AIDS Rep. 2014;11:279–290. [PubMed: 24966138]
3. Wallace LMK, Ferrara M, Brothers TD, et al. Lower frailty is associated with successful cognitive aging among older adults with HIV. AIDS Res Hum Retroviruses 2017;33:157–163. [PubMed: 27869500]
4. Fried LP, Tangen CM, Walston J, et al. Frailty in older adults: evidence for a phenotype. J Gerontol A Biol Sci Med Sci. 2001;56:M146–M156. [PubMed: 11253156]
5. Paul RH, Cooley SA, Garcia-Egan PM, et al. Cognitive performance and frailty in older HIV-positive adults. J Acquir Immune Defic Syndr. 2018; 79:375–380. [PubMed: 29957675]
6. Morgello S, Gensler G, Sherman S, et al. Frailty in medically complex individuals with chronic HIV. AIDS. 2019;33:1603–1611. [PubMed: 31305330]
7. Greene M, Covinsky KE, Valcour V, et al. Geriatric syndromes in older HIV-infected adults. J Acquir Immune Defic Syndr. 2015;69:161–167. [PubMed: 26009828]
8. Antinori A, Arendt G, Becker JT, et al. Updated research nosology for HIV-associated neurocognitive disorders. Neurology. 2007;69: 1789–1799. [PubMed: 17914061]
9. Miller PJ, Lubke GH, McArtor DB, et al. Finding structure in data using multivariate tree boosting. Psychol Methods. 2016;21:583–602. [PubMed: 27918183]
10. Luckett P, Paul RH, Navid J, et al. Deep learning analysis of cerebral blood flow to identify cognitive impairment and frailty in persons living with HIV. J Acquir Immune Defic Syndr. 2019;82:496–502. [PubMed: 31714429]
11. Beck AT, Steer RA, Brown GK. Manual for the Beck Depression Inventory-II. San Antonio, TX: Psychological Corporation; 1996.
12. Reitan RM, Davison LA. Clinical Neuropsychology: Current Status and Applications. Oxford, England: V. H. Winston & Sons; 1974.
13. Wechsler D Wechsler Adult Intelligence Scale. San Antonio, TX: Psychological Corporation; 1997.
14. Matthews CG, Klove K. Instruction Manual for the Adult Neuropsychology Test Battery. Madison, WI: University of Wisconsin Medical School; 1964.
15. Benedict RHB, Schretlen D, Groninger L, et al. Hopkins verbal learning test—revised: normative data and analysis of inter-form and test-retest reliability. Clin Neuropsychol. 1998; 12:43–55.

16. Benedict RHB. Brief Visuospatial Memory Test-Revised BVMT-R. Lutz, FL: Psychological Assessment Resources, Inc; 1997.
17. Delis DC, Kaplan E, Kramer JH. Delis-Kaplan Executive Function System (D-KEFS). San Antonio, TX: Psychological Corporation; 2001.
18. Piatt AL, Fields JA, Paolo AM, et al. Action (verb naming) fluency as an executive function measure: convergent and divergent evidence of validity. Neuropsychologia. 1999;37:1499–1503. [PubMed: 10617270]
19. Borkowski JG, Benton AL, Spreen O. Word fluency and brain damage. Neuropsychologia. 1967;5:135–140.
20. Goodglass H, Kaplan E, Barresi B. The Assessment of Aphasia and Related Disorders. Philadelphia, PA: Lippincott Williams & Wilkins; 2001.
21. Gladsjo JA, Schuman CC, Evans JD, et al. Norms for letter and category fluency: demographic corrections for age, education, and ethnicity. Assessment. 1999;6:147–178. [PubMed: 10335019]
22. Norman MA, Moore DJ, Taylor M, et al. Demographically corrected norms for African Americans and Caucasians on the Hopkins Verbal Learning Test–Revised, Brief Visuospatial Memory Test–Revised, Stroop Color and Word Test, and Wisconsin Card Sorting Test 64-Card Version. J Clin Exp Neuropsychol. 2011;33:793–804. [PubMed: 21547817]
23. Tanenbaum AB, Snyder AZ, Brier MR, et al. A method for reducing the effects of motion contamination in arterial spin labeling magnetic resonance imaging. J Cereb Blood Flow Metab. 2015;35:1697–1702. [PubMed: 26036937]
24. Brier MR, Thomas JB, Fagan AM, et al. Functional connectivity and graph theory in preclinical Alzheimer's disease. Neurobiol Aging. 2014;35.
25. Gholipour A, Kehtarnavaz N, Briggs RW, et al. A field map guided approach to non-rigid registration of brain EPI to structural MRI. Proc SPIE Int Soc Opt Eng. 2007;6512.
26. Power JD, Barnes KA, Snyder AZ, et al. Spurious but systematic correlations in functional connectivity MRI networks arise from subject motion. Neuroimage. 2012;59:2142–2154. [PubMed: 22019881]
27. Fischl B. Freesurfer. Neuromage. 2012;62:774–781.
28. Paul RH, Cho KS, Belden AC, et al. Machine learning classification of neurocognitive performance in children with perinatal HIV initiating de novo antiretroviral therapy. AIDS. 2020;34:737–748. [PubMed: 31895148]
29. Papini S, Pisner D, Shumake J, et al. Ensemble machine learning prediction of posttraumatic stress disorder screening status after emergency room hospitalization. J Anxiety Disord. 2018;60:35–42. [PubMed: 30419537]
30. Riedel BC, Daianu M, Ver GS, et al. Uncovering biologically coherent peripheral signatures of health and risk for Alzheimer's disease in the aging brain. Front Aging Neurosci. 2018;10:390. [PubMed: 30555318]
31. Pedregosa F, Varoquaux G, Michel V, et al. Scikit-learn: machine learning in Python. JMLR. 2011;12:2825–2830.
32. Jiangchun L SauceCat/PDPbox. GitHub 2008 Available at: https://github.com/SauceCat/PDPbox. Accessed November 5, 2019.
33. Valverde-Albacete FJ, Peláez-Moreno C. 100% classification accuracy considered harmful: the normalized information transfer factor explains the accuracy paradox. PLoS One. 2014;9:e84217. [PubMed: 24427282]
34. Xia M, Wang J, He Y. BrainNet Viewer: a network visualization tool for human brain connectomics. PLoS One 2013;8:e68910. [PubMed: 23861951]
35. Paul R, Cohen R, Navia B, et al. Relationships between cognition and structural neuroimaging findings in adults with human immunodeficiency virus type-1. Neurosci Biobehavioral Rev. 2002;26:353–359.
36. Molnar-Szakacs I, Iacoboni M, Koski L, et al. Functional segregation within pars opercularis of the inferior frontal gyrus: evidence from fMRI studies of imitation and action observation. Cereb Cortex. 2005;15: 986–994. [PubMed: 15513929]
37. Ances BM, Sisti D, Vaida F, et al. Resting cerebral blood flow. Neurology. 2009;73:702–708. [PubMed: 19720977]

38. Ances BM, Ortega M, Vaida F, et al. Independent effects of HIV, aging, and HAART on brain volumetric measures. J Acquir Immune Defic Syndr. 2012;59:469–477. [PubMed: 22269799]
39. Seitzman BA, Snyder AZ, Leuthardt EC, et al. The state of resting state networks. Top Magn Reson Imag. 2019;28:189–196.
40. Zayyad Z, Spudich S. Neuropathogenesis of HIV: from initial neuro-invasion to HIV-associated neurocognitive disorder (HAND). Curr HIV/AIDS Rep. 2015;12:16–24. [PubMed: 25604237]
41. Spudich S, Robertson KR, Bosch RJ, et al. Persistent HIV-infected cells in cerebrospinal fluid are associated with poorer neurocognitive performance. J Clin Invest. 2019;129:3339–3346. [PubMed: 31305262]
42. Crepaz N, Tang T, Marks G, et al. Durable viral vuppression and transmission risk potential among persons with diagnosed HIV infection: United States, 2012–2013. Clin Infect Dis. 2016;63:976–983. [PubMed: 27358354]
43. Marks G, Gardner LI, Rose CE, et al. Time above 1500 copies: a viral load measure for assessing transmission risk of HIV-positive patients in care. AIDS. 2015;29:947–954. [PubMed: 25768835]

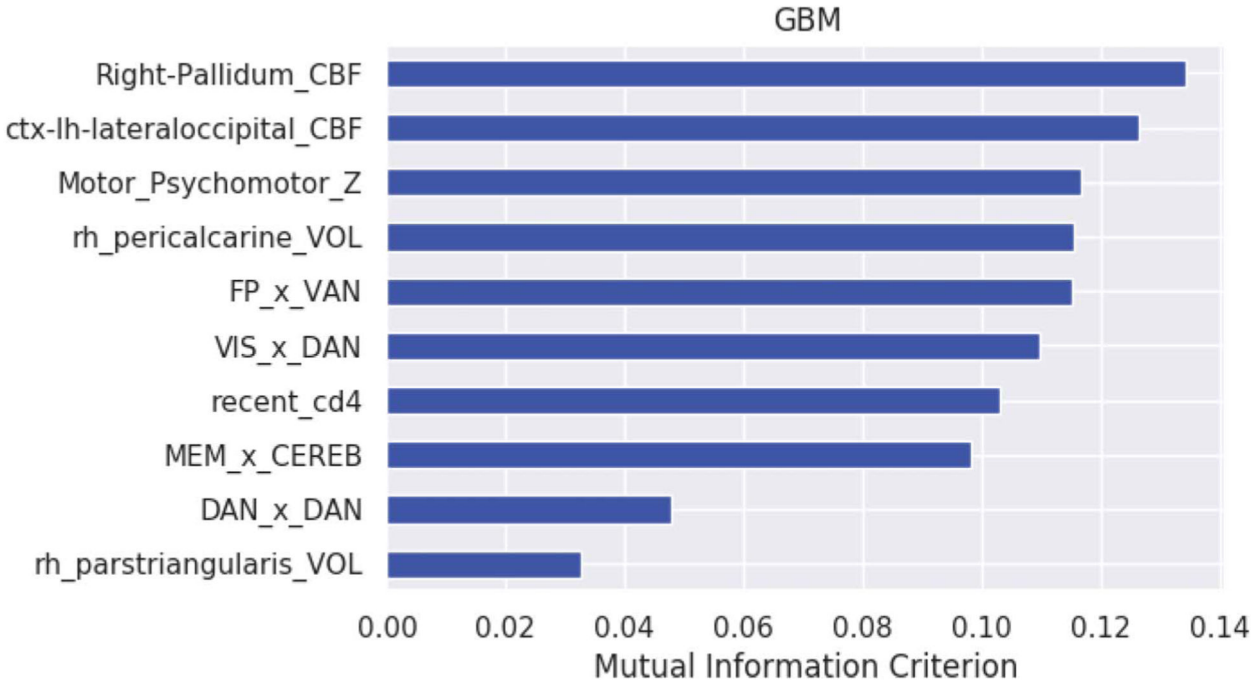


**Figure 1.**

Feature importance for the linear GBM. Feature importance by rank order. Right pallidal CBF (Right-Pallidal_CBF), left lateral occipital CBF (ctx-lh-lateraloccipital_CBF), psychomotor Z score (Motor_Psychomotor_Z), right pericalcarine volume (rh_pericalcarine_Vol), frontoparietal x ventral attention connectivity (FP_x_VAN), visual x dorsal attention connectivity (VIS_x_DAN), recent_CD4 T-cell count, memory_x_cerebellum connectivity (MEM_x_CEREB), dorsal attention (DAN) intranetwork connectivity, and right pars triangularis volume (rh_parstrianularis_VOL).

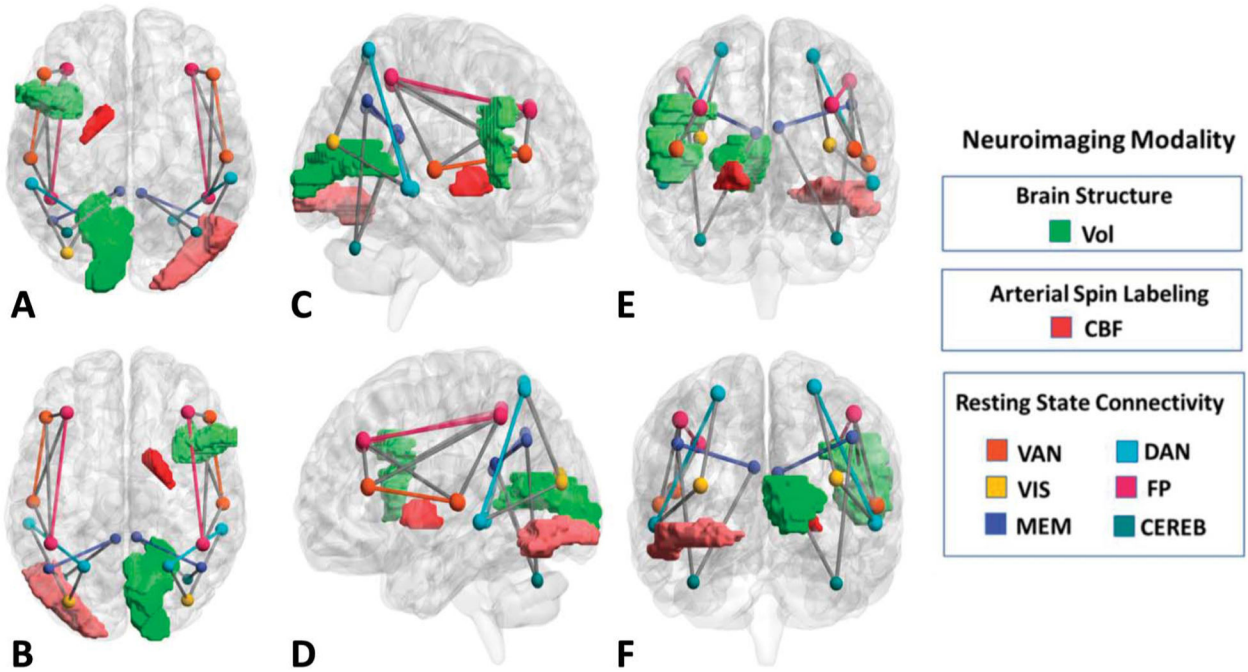


**FIGURE 2.**

Volumetric, resting-state connectivity, and blood flow signatures of frailty in persons living with HIV. Brain regions and networks associated with frailty identified in the linear GBM from superior (A), inferior (B), right hemisphere (C), left hemisphere(D), rostral (E), and caudal (F) perspectives. Darker shades of color represent a higher rank order (mutual information criterion) of the individual feature. Image created using BrainNet Viewer [43].

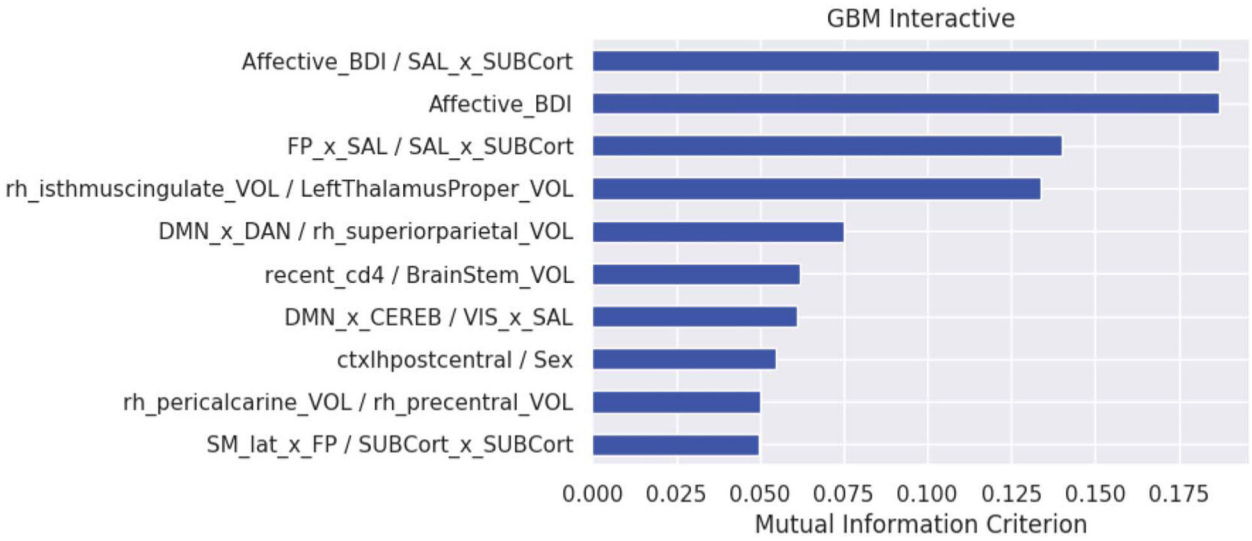


**FIGURE 3.**

Feature importance for the GBM allowing for 2-way interactions. Feature importance by rank order. Beck Depression Inventory-II and salience x subcortical region connectivity (Affective_BDI/SAL_x_SUBCort), affective BDI-II (Affective_BDI), FP × salience and salience × subcortical connectivity (FP_x_SAL/SAL_x_SUBCort), right isthmus cingulate volume and left thalamic volume (rh_isthmuscingulate_VOL/LeftThalamusProper_VOL), default mode x dorsal attention connectivity and superior parietal volume (DMN_x_DAN/rh_superiorparietal_VOL), recent CD4/brainstem volume (recent_cd4 Brainstem_VOL), default mode x cerebellum connectivity and visual x salience connectivity (DMN_x_CEREB/VIS_x_SAL), left postcentral cortex volume and female sex (ctxlh-postcentral_Sex), right pericalcarine volume and right precentral volume (rh_pericalcarine_VOL/rh_precentral_VOL), and sensorimotor region × FP connectivity and subcortical intranetwork connectivity (SM_lat_x_FP/SUBCort_x_SUBCort).

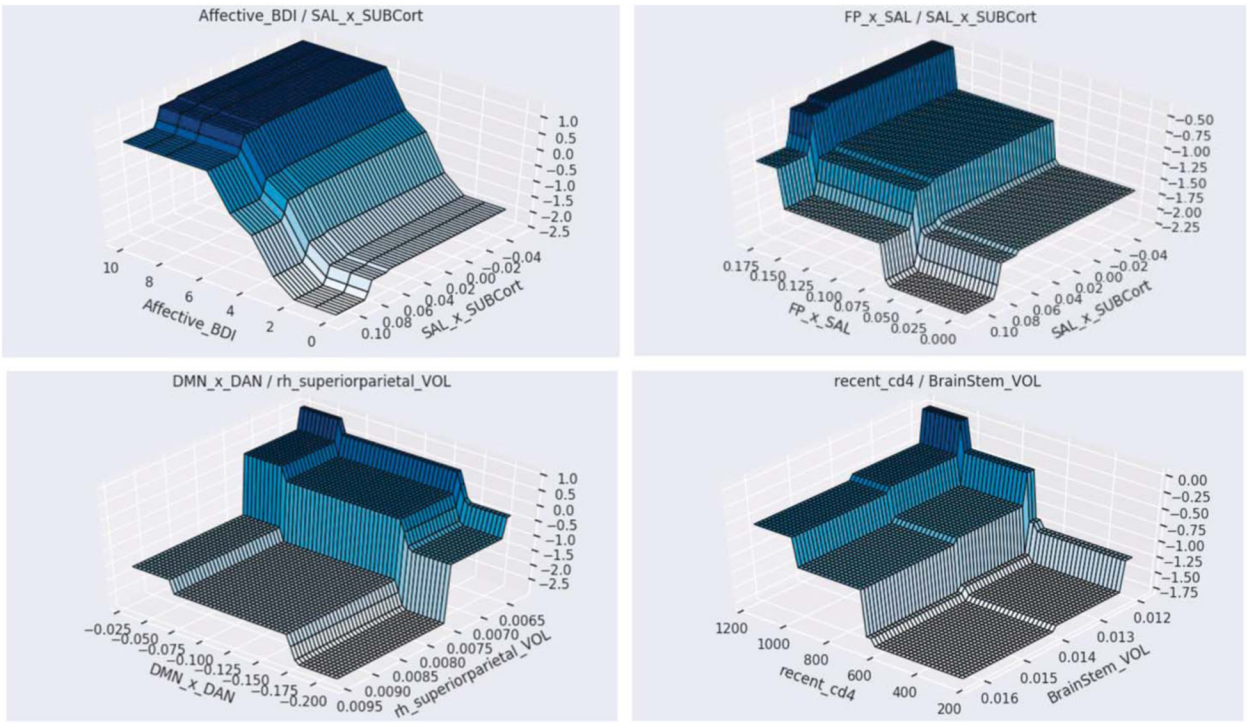


**FIGURE 4.**

Surface plots depicting 2-way interactions. 3-D graphs of the 2-way interactions. Top left: higher BDI-II affective score and lower salience (SAL) and SUB; top right: higher FP × SAL connectivity and lower SAL × SUB connectivity; bottom left: higher volume of the right superior parietal region and lower default mode (DMN) · dorsal attention (DAN) connectivity; bottom right: higher recent CD4 and lower brainstem volume.

**TABLE 1.**

Demographic and Clinical Characteristics

| Variable | Frail (n = 20) | Nonfrail (n = 85) | *P* |
|---|---|---|---|
| Demographic | | | |
| Age (yrs) (SD) | 55.2 (8.31) | 55.8 (7.26) | 0.76 |
| Sex (% male/female) | 70% | 88% | **0.04** |
| Race (% African American) | 70% | 58% | 0.11 |
| Education (yr) (SD) | 12.5 (2.53) | 13.6 (2.7) | 0.11 |
| HIV disease | | | |
| Duration of HIV infection (mo) (SD) | 214 (85) | 209 (107) | 0.83 |
| Undetectable viral load (<50 copies/mL), % | 85% | 91% | |
| Current CD4 count (cells/$mm^3$), median (IQR) | 688 (348.9) | 528 (248.9) | **0.02** |
| Nadir CD4 count (cells/$mm^3$), median (IQR) | 230 (200.0) | 91 (182.36) | 0.05 |
| Health comorbidities | | | |
| Affective BDI-II subscale (SD) | 4.0 (2.9) | 1.7 (2.0) | **0.003** |
| Hepatitis C coinfection, % | 25% | 12% | 0.13 |
| Neurocognitive performances | | | |
| Global: mean (SD) | −0.44 (0.7) | −0.25 (0.6) | 0.22 |
| Executive function: mean (SD) | −0.54 (0.7) | −0.33 (0.7) | 0.21 |
| Psychomotor/Processing speed: mean (SD) | −0.31 (0.8) | 0.02 (0.7) | 0.07 |
| Memory: mean (SD) | −0.71 (1.1) | −0.39 (0.9) | 0.19 |
| Learning: mean (SD) | −0.76 (1.0) | −0.53 (0.9) | 0.33 |
| Language: mean (SD) | 0.12 (1.0) | −0.04 (0.8) | 0.47 |

Bold indicates $P < 0.05$.

IQR, interquartile rating.